Journal of
Materials Chemistry C

PAPER

View Article Online
View Journal | View Issue

Published on 03 November 2015. Downloaded by Harvard University on 19/11/2015 15:08:36.

Cite this: J. Mater. Chem. C, 2015, 3, 12098

Direct-liquid-evaporation chemical vapor deposition of smooth, highly conformal cobalt and cobalt nitride thin films†

Jing Yang,[a] Kecheng Li,[a] Jun Feng[b] and Roy G. Gordon*[ab]

Received 8th October 2015,
Accepted 2nd November 2015

DOI: 10.1039/c5tc03221k

www.rsc.org/MaterialsC

By a direct-liquid-evaporation chemical vapor deposition (DLE-CVD) method, we deposited smooth low-resistance cobalt (Co) and cobalt nitride (Co_xN) thin films with excellent conformality at low temperatures down to 200 °C. In the DLE process, a cobalt amidinate precursor solution, bis(*N*,*N*′-diisopropylacetamidinato)cobalt(II) dissolved in tetradecane, was vaporized as it flowed smoothly, without boiling, inside heated tubing. This DLE process avoids creating unwanted particles that are generated when droplets from a nebulizer evaporate in a conventional direct-liquid-injection (DLI) process. The vapor then mixed with ammonia (NH_3) and hydrogen (H_2) and flowed over substrates in a tubular CVD reactor, resulting in metallic Co or Co_xN films by tuning the NH_3/H_2 co-reactant ratio. This process deposited pure and highly conformal Co or Co_xN films in trenches with 60 : 1 or 45 : 1 aspect ratio respectively. The good conformality is crucial towards realizing potential applications, such as in 3D contacts and interconnects in microelectronics.

Introduction

Thin films of cobalt (Co) and cobalt nitride (Co_xN) have attracted considerable attention for their applications in giant magnetoresistance (GMR) devices,[1–3] spintronics,[4] and microelectronics technology.[5,6] For example, Co,[5] Co_xN,[7] or Co-based alloy[8,9] have proven to be effective adhesion layers in copper interconnects as they demonstrated enhanced bonding between copper and barrier layers. Co has also been used as a wetting layer to induce void-free filling of narrow copper lines by reflow of non-conformal PVD copper for sub-20 nm nanostructures.[10] $CoSi_2$, fabricated by the reaction of Co with silicon, is a useful material for contacts due to its thermal and chemical stability.[11,12]

Cobalt and cobalt nitride have been previously deposited by various means, including physical vapor deposition (PVD),[2,4] chemical vapor deposition (CVD)[7–9,12–18] and atomic layer deposition (ALD)[5,6,8,9,19–21] methods. As microelectronics and magnetic-storage devices continue to shrink in dimensions,[22] highly conformal metal deposition is required for further downsizing and for the construction of ultra large scale integration (ULSI) with three dimensional structures. In these applications, the poor step coverage of PVD methods causes severe limitations, while CVD[8] and ALD[5] are favored as they are able to produce high-quality and conformal thin films.

By thermal ALD using Co(^{i}Pr-MeAMD)$_2$ (bis(*N*,*N*′-diisopropylacetamidinato)cobalt(II)) precursor and H_2[5] or NH_3[20] co-reactants, successful deposition of high quality cobalt films has been realized at temperatures between 260 °C and 350 °C. The films exhibited resistivity ranging from 46 to 200 μΩ cm and excellent step coverage,[5] coating holes with a 40 : 1 aspect ratio conformally.

However, the growth rate of the ALD-Co[5] is less than 0.1 nm min^{-1}, which is slow compared to CVD methods. In contrast, direct-liquid-injection (DLI)-CVD[17,23] provides much faster growth rates. It has the advantage of effective prevention of precursors' early decomposition as compared to the traditional bubbler delivery since the precursor is typically stored at room temperature.[24] Furthermore, this technique can be applied to a wide range of precursors, even those having low vapor pressure and/or limited thermal stability. DLI-CVD can deliver high vapor concentrations of precursors that are hard to achieve by conventional bubbler delivery, which is favorable for growing highly conformal films with high growth rates. DLI-CVD has been employed to deposit Ni,[16,23,25] Co,[16] cobalt oxide,[26] Ag,[16,27] Ru,[28] Cu,[16,29] and metal oxides (high-*k*).[30] The DLI-CVD method typically employs a nebulizer to break up the liquid solution into tiny droplets, which then generate vapor when the droplets contact a hot carrier gas.[16] However this method is limited

[a] *School of Engineering, Applied Sciences, Harvard University, Cambridge, MA 02138, USA*
[b] *Department of Chemistry and Chemical Biology, Harvard University, Cambridge, MA 02138, USA. E-mail: gordon@chemistry.harvard.edu*

† Electronic supplementary information (ESI) available: Electron Diffraction (ED) images and results for DLE-CVD Co and Co_xN films, Arrhenius plot of the Co growth rate, deposition rate and sheet resistance as a function of the cobalt precursor delivery rate, and an X-ray Reflection (XRR) measurement of film thickness. See DOI: 10.1039/c5tc03221k

This journal is © The Royal Society of Chemistry 2015

Published on 03 November 2015. Downloaded by Harvard University on 19/11/2015 15:08:36.

because it also produces small particles made up of non-volatile residues in the precursor after most of the precursor has evaporated. These particles can be carried along with the vapor into the deposition region, where they can contaminate substrates. Particles are a serious problem in microelectronics, where they can cause defects. Particles can also accumulate in the very narrow openings of a nebulizer and block the liquid flow. Blockage of a vaporizer can also arise if a highly volatile solvent evaporates more quickly than a solid precursor.

Here we use a direct-liquid-evaporation (DLE) CVD method for Co and Co_xN deposition. This DLE-CVD method vaporizes the precursor solution by flowing the liquid along a tubing coil inside an oven.[31] It takes advantage of the rapid heat transfer from a heated solid tube to the flowing liquid, which is faster than the heat transfer from a heated carrier gas to liquid droplets. Any non-volatile residue left by DLE tends to adhere to the bottom inside the tube, where it will remain instead of being carried into the reactor along with the vapors. And the inexpensive tubing coil could be cleaned or replaced before the residue builds up over a long period of time. Because the opening in the DLE tubing is much larger than the tiny nozzles in a DLI nebulizer, the tubing does not become clogged or blocked easily. Our DLE-CVD system has demonstrated consistent performance over years of operation[23,25] without any need to replace the tubing coil. This system avoids the particle contamination generated by DLI-CVD methods, while preserving its advantages of high growth rate, conformal coating, and reproducible generation of known concentrations of precursor vapor.

For Co CVD processes, the choice of a suitable cobalt precursor is crucial to obtain high-quality cobalt or cobalt nitride films. Inorganic cobalt precursors, such as cobalt halides, have very low volatility and would require very high evaporation temperatures,[32] which renders them unsuitable for CVD. Therefore, cobalt thin film deposition is typically carried out using various metalorganic precursors. Co can be deposited from thermal decomposition of $Co_2(CO)_8$[11,15,33] at substrate temperature ranging from 50 °C to 200 °C. However there are undesirable, but kinetically favourable, reaction pathways that compete with the deposition of pure Co, including polymerization of the precursor and formation of unstable $HCo(CO)_4$.[15] Co deposition from cobalt carbonyl complexes,[18] $CoCp_2$[11,13,19,21] or $Co(acac)_2$[12,17] typically require relatively high reaction temperatures above 250 °C and produce cobalt with significant amounts of impurities, including carbon and oxygen.

Herein, we chose $Co(^{i}Pr\text{-}MeAMD)_2$ as the Co precursor because this cobalt amidinate[5,20] can form highly pure and conformal cobalt and cobalt nitride films. We investigated the impact of different processing parameters and found the optimal conditions for producing highly-conformal, high-quality Co and Co_xN films by DLE-CVD. From quantum chemical calculations, it was found that NH_3 can effectively lower the activation energy of cobalt-based thin film deposition from amidinate precursors compared with H_2 as the only reducing agent.[8] Using a mixture of NH_3 and H_2, we successfully deposited highly conductive, pure metallic cobalt films at 200 °C. The as-deposited Co film has excellent step coverage in trenches with 60 : 1 aspect ratio. On the other hand, using NH_3 as the only co-reactant in the deposition, we demonstrated the formation of hexagonal Co_3N conformally coating 45 : 1 aspect ratio trenches. The growth rates are much higher than those obtained by ALD processes. The highly conformal Co and Co_3N films are promising materials for applications in next-generation microelectronic devices, as well as for conformal cobalt films for other uses, such as catalysts.

Experimental section

Precursor solution

The cobalt precursor is $Co(^{i}Pr\text{-}MeAMD)_2$, bis(*N*,*N*′-diisopropylacetamidinato)cobalt(II), ($CoC_{16}H_{34}N_4$) (Dow Chemical Company). The synthesis of this cobalt amidinate has been reported previously.[34,35] The cobalt precursor is a dark green, air-sensitive solid in room temperature, with a melting point of 84 °C. This solid precursor has a vapor pressure of ~30 mTorr at 40 °C.[34] Tetradecane $C_{14}H_{30}$ (olefin free, ≥99.0% (GC), Sigma-Aldrich Co.) was used to dissolve the cobalt precursor. The tetradecane solvent was purified of water and other impurities by distillation from sodium.

The cobalt precursor solution was prepared in a glovebox by dissolving 5 grams of ($Co(^{i}Pr\text{-}MeAMD)_2$) in 50 ml $C_{14}H_{30}$ (tetradecane), forming a 0.38 molal (moles of solute per kg of solvent), 12 wt% solution. The precursor solution was transferred into a glass container inside the glovebox. The solution was kept at room temperature and was pressurized by pure helium (He) at pressure of 20 psi or above. Helium was chosen as the push gas in order to minimize the dissolved gas in the solution, to prevent gas bubbles from destabilizing the liquid flow controller.

DLI-CVD of cobalt-based thin films

In preliminary experiments, a Brooks Instrument nebulizer was initially used in a DLI process by breaking up the fluid into small micron-sized droplets before contacting a hot carrier gas. This DLI process, however, produced particles on the substrates. Also, the nebulizer was vulnerable to even slight contamination and easily got clogged in the narrow opening with 0.02'' inner diameter that was used to break up the fluid into droplets. DLI systems made by MKS Instruments and by Horiba were also tested in our laboratory and abandoned because of particle generation and clogging.

DLE-CVD of cobalt-based thin films

The flow of the precursor solution was controlled by Brooks Instrument's Quantim QMBC Coriolis flow controllers at adjustable flow rates up to 20 g h^{-1}. The typical cobalt precursor solution flow rate was set at 5 g h^{-1}. An advantage of this flow controller is that it sets a true mass flow rate independently of any other physical properties of the solution, such as its viscosity, density or thermal conductivity. It is calibrated once with any liquid, and the same calibration applies to any other liquid or solution. The flow of precursor solution was mixed with a 100 sccm flow of N_2 gas at room temperature in a tee.

Published on 03 November 2015. Downloaded by Harvard University on 19/11/2015 15:08:36.

This mixture of the liquid solution and gas then flowed down into a coil of stainless steel tubing kept at 180 °C in an oven, where the precursor solution quickly vaporized. The vaporization temperature was chosen to be 150 °C or above in order to evaporate the solution completely and quickly; 130 °C was too low to fully vaporize the solution. Depositions at 150 °C and 180 °C showed similar growth rate, indicating 150 °C was sufficient to evaporate the precursor completely. A similar vaporizer design has been described elsewhere.[31] The vapor mixture exiting from the DLE vaporizing coil was then mixed with reducing agents H_2 and/or NH_3 just before entering the custom-built tubular hot-wall reactor. The substrates were supported on a stainless steel half-cylinder inserted into the reactor tube. A heating element and a thermocouple were embedded in the half-cylinder to control the deposition temperature. The substrates were typically held at temperatures of 200–240 °C and heated 10 to 20 °C higher than the reactor wall temperature to decrease the rate of deposition on the reactor walls. The deposition pressure was set at 10 Torr using an MKS pressure controller. The co-reactant gas flow rates were controlled by mass flow controllers (MKS Instruments), and the sum of the NH_3 and H_2 flow rates was typically held at 200 sccm. The ratio of NH_3 and H_2 was tuned to adjust the film composition. Table 1 summarizes the fabrication conditions of the DLE-CVD Co/Co_xN films. The schematic diagram of the DLE-CVD apparatus is shown in the ESI.†

Thermally oxidized silicon wafers, glassy carbon, and Si_3N_4 membranes (TEM grids from Ted Pella, Inc. 15 nm Si_3N_4 membrane with 0.25 × 0.25 mm aperture on 200 μm Si.) were used as substrates. The substrates were treated by UV/ozone cleaner (Samco model UV-1, wavelengths = 185 nm and 254 nm) for 5 minutes at the room temperature to remove organic contaminants.

Characterization

The sheet resistance of the as-deposited films on silicon oxide was measured by a four-point probe station (Veeco Instruments, Model FPP-5000 or Miller Design & Equipment, Model FPP-5000). The thicknesses of the films were measured by Field Emission Scanning Electron Microscope (FESEM; Zeiss FESEM Ultra Plus) and X-ray reflectometry (XRR). The crystalline phases were evaluated by transmission electron microscopy (TEM; JEOL 2100 TEM system). The compositions of the films were determined by Rutherford backscattering spectroscopy (RBS), X-ray fluorescence (XRF; SPECTRO XEPOS III), X-ray photoelectron spectroscopy (XPS; ESCA Model SSX-110) and atom probe tomography (APT; CAMECA LEAP 4000X HR). The surface roughness of the films was evaluated by atomic force microscopy (AFM; Asylum MFP-3D AFM system).

Table 1 Experimental conditions of DLE-CVD of cobalt or cobalt nitride

DLE-CVD parameters	Cobalt/cobalt nitride
Solvent	Tetradecane ($C_{14}H_{30}$)
Concentration	0.38 molal/12 wt%
Temperature of Co precursor solution reservoir	Room temperature
Flow rate of Co precursor solution	5 g h^{-1} (5 to 20 g h^{-1})
Temperature of vaporizing stainless steel coil	180 °C (150 to 180 °C)
Flow rate of carrier gas N_2	100 sccm
Flow rates of co-reactants NH_3 + H_2	10 + 190, 20 + 180, 50 + 150, 100 + 100, 150 + 50, 200 + 0 sccm
Substrate temperature	200 °C (200 to 240 °C)
Deposition total pressure	10 Torr

Results and discussions

Direct-liquid-evaporation chemical vapor deposition (DLE-CVD) of cobalt nitride and cobalt metal

We deposited either pure metallic cobalt or cobalt nitride by DLE-CVD at substrate temperatures near 200 °C.

To deposit cobalt nitride, ammonia was used as the only co-reactant gas, flowing at 200 sccm. Combined with 5 g h^{-1} of precursor solution and 100 sccm of N_2 carrier gas, the molar percentages and partial pressures of the gas mixture introduced into the reactor were 0.2% or 0.02 Torr Co precursor vapor, 2.8% or 0.28 Torr tetradecane, 65% or 6.5 Torr NH_3 and 32% or 3.2 Torr N_2. RBS measurements determined the cobalt to nitrogen atomic ratio of the as-deposited cobalt nitride films to be around 3 : 1, as shown in Fig. 1(a). The XPS depth-profile in Fig. 1(c) also showed significant N (~23 at%) in the cobalt nitride films. In addition, no C and O were detected by XPS inside the film, which indicated the film had less than about 1% of these impurities. However, the XPS cannot detect concentrations below the detection limit (~1 at%). Atom probe tomography (APT) provides 3-D compositional images at the atomic scale with very high sensitivity (ppm). An APT specimen was prepared by coating a thin layer of cobalt nitride film (~30 nm) onto pre-sharpened Si microtips (tip radius ~20 nm, with semi-angle ~8°). Fig. 2 revealed the 3D atom mapping of Co and N atoms inside the film, which showed that Co and N atoms are uniformly distributed. The average concentrations of C and O impurities were determined to be 0.4 at% and 0.2 at%, respectively. This result agreed with the XPS depth-profile that the cobalt nitride films contained very low levels of impurities.

When using H_2 as the only co-reactant for the DLE-CVD cobalt deposition, the growth rate is very slow ($\ll$0.5 nm min^{-1}) at 300 °C or lower. The cobalt film deposited at 310 °C contained a significant amount of carbon (~30 at%) inside the film, as determined by an XPS depth-profile. The carbon could be attributed to thermal decomposition of the cobalt precursor at that high substrate temperature.

When NH_3 is used as a co-reactant along with H_2, the process deposits a pure cobalt metal film, containing neither carbon nor nitrogen. For films deposited using both NH_3 and H_2 with different feed ratios listed in Table 2, XPS depth-profile studies did not detect any impurities (<1 at% C or N). As shown in Fig. 1(d), the XPS analysis of the cobalt film deposited from a mixture of 100 sccm H_2 and 100 sccm NH_3 shows no N 1s peak after Ar sputtering for 1 min, indicating the N content in the film is below the detection limit. The RBS result in Fig. 1(b) also confirmed this conclusion, with N content below the noise level. Atom probe tomography (APT) revealed the

 This journal is © The Royal Society of Chemistry 2015

Published on 03 November 2015. Downloaded by Harvard University on 19/11/2015 15:08:36.

Fig. 1 RBS spectra of (a) DLE-CVD Co_3N film and (b) Co films deposited at 200 °C on a glass carbon substrate. Insets are close-up view of regions corresponding to C, N and O elements. (c) XPS survey of (1) DLE-CVD Co_3N deposited at 200 °C, (2) after 1 min Ar sputtering, (3) after 5 min Ar sputtering. (d) XPS survey of (1) DLE-CVD Co deposited at 200 °C, (2) after 1 min Ar sputtering, (3) after 4 min Ar sputtering.

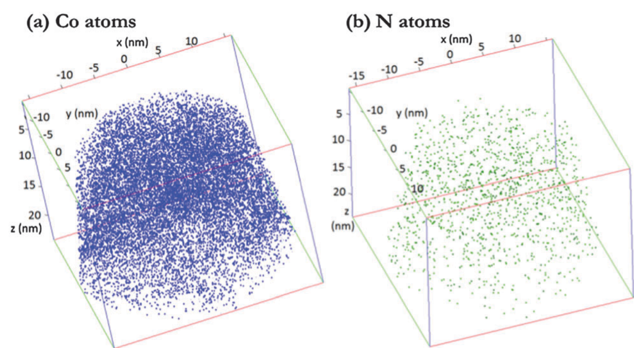

Fig. 2 3D compositional maps of (a) Co (blue), (b) N (green) atoms in the as-deposited cobalt nitride films. (For visualization reasons, only 5% of detected Co, N atoms are illustrated in the reconstructed 3D-atom maps.)

N content inside the cobalt film is below 0.1%. The APT data, along with the XPS and RBS results, prove that the deposited cobalt films have very high purity. The H_2 effectively removed nitrogen from the film during the deposition process. The existence of carbon and oxygen on the surface is due to surface oxidation of the films upon exposure to air. Oxygen contamination at the surface is not surprising as the Co surface will be oxidized upon exposure to the atmosphere.[36]

The mechanism by which NH_3 promotes the growth of pure cobalt at a low temperature was studied by the Shimogaki[8] and Gordon[37] groups, who calculated the activation energy for different reaction pathways between cobalt amidinate precursors and H_2 or NH_3. They found that NH_3 is effective in lowering the activation energy of the deposition process compared to H_2. Our experiments agreed with these results. With 10 sccm NH_3 and 190 sccm H_2 (*i.e.* only 5% of the reducing agent is NH_3), the growth rate at 200 °C reached $\sim$2 nm min^{-1}. In contrast, no film is deposited at this temperature (200 °C) with H_2 as the only co-reactant. This suggests that NH_3 adsorbed on the substrate surface might enable the chemisorption of the cobalt amidinate precursor by reaction with N–H bonds on the surface. As shown in Table 2, the deposition rate varied somewhat with different

Published on 03 November 2015. Downloaded by Harvard University on 19/11/2015 15:08:36.

Table 2 The crystalline phase of Co, Co_xN thin films deposited at 200 °C by a varied ratio of NH_3/H_2 as co-reactants, and their corresponding electrical resistivity, deposition rate and the step coverage

NH_3 (sccm)	H_2 (sccm)	Phase	Resistivity (μΩ cm)	Deposition rate (nm min^{-1})	Aspect ratio of hole patterns with ~100% step coverage
0	200			0	
20	180	fcc-Co	~50	~2	~10:1
50	150	fcc & hcp-Co	~50	~2	~20:1
100	100	fcc & hcp-Co	~25	~1 to 2	~50:1
150	50	fcc & hcp-Co	~100	~2	~20:1
200	0	hcp-Co_3N	~160	~1	~45:1

combinations of co-reactants. Deposition at 10 torr and 200 °C, with 100 sccm NH_3 and 100 sccm H_2 produced pure cobalt film growth with the best uniformity, with a growth rate between 1 and 2 nm min^{-1}, as determined by XRR (see Table 3 and ESI,† Fig. S4).

The crystalline phases of the as-deposited thin films evolved as the NH_3 concentration increased in the co-reactant. When using 20 sccm NH_3 and 180 sccm H_2 as co-reactants, the diffraction peaks correspond to the cubic Co phase (111), (200), (220), and (311) peaks (see ESI,† Table S1). The electron diffraction (ED) patterns (Fig. 3) show that with increasing NH_3 concentration, the crystalline phase of the film evolved from purely face-cubic-center (fcc) β-Co to a mixed fcc β-Co and hexagonal-close-packed (hcp) α-Co phase. As the NH_3 ratio increases, smaller amounts of diffraction peaks corresponding to hexagonal Co phase (see ESI,† Tables S2 to S4) start to appear, with the major diffraction peaks corresponding to the cubic Co phase. The hcp α-Co (100), (101), and (102) gradually become more evident along with the dominant fcc Co peaks as shown in Fig. 3(b) and (c). When NH_3 became the only co-reactant, the deposited films consisted primarily of the polycrystalline Co_3N with a hexagonal phase, as shown by the ED image (Fig. 3(d)). The diffraction rings correspond to hexagonal Co_3N (100), (002), (101), (102), (110), (103), and (112), respectively (ESI,† Table S5). Although hcp Co is the stable crystalline phase at temperatures up to about 450 °C, metastable fcc Co has also been observed in both PVD[38–40] and CVD-Co[14,32,36] films deposited at lower temperatures as reported by several other groups. This is because the crystal structure of cobalt thin films can be influenced by many factors besides the growth temperature, such as the substrate,[36] the presence of seeding layers,[13] the grain size,[14] and the film thickness.[32]

The densities of as-deposited Co and Co_3N films were determined by combining the XRR thickness and the RBS areal density. For Co films deposited with low concentration of NH_3 and high concentration of H_2, the density was around 8.6 g cm^{-3}, close to the bulk Co density of 8.9 g cm^{-3}. The Co_3N film deposited with 200 sccm NH_3 showed a lower density of 5.5 g cm^{-3}. The deposited Co_3N has a relatively low density compared to calculated Co_3N density, 7.9 g cm^{-3} (see hcp Co_3N PDF Card No. 06-0691).

The resistivity of Co/Co_3N films was affected by the deposition condition, in particular, the feed ratio of co-reactants, listed in Table 2. Cobalt films deposited with 100 sccm NH_3 and 100 sccm H_2 showed the lowest resistivity. A 45 nm-Co film had a resistivity around ~28 μΩ cm, whereas bulk cobalt crystal resistivity is around 6.2 μΩ cm. A 15 nm-Co_3N film had a higher resistivity of ~160 μΩ cm, which is similar to a reported CVD-Co_xN[7] value of 180 μΩ cm.

The surface morphologies of Co and Co_xN films using different co-reactant combinations were examined by SEM, as shown in Fig. 4. The grain size of Co deposited using 10 sccm NH_3 and 190 sccm H_2 is largest among all the different growth conditions. As the ammonia flow rate increases from 10 sccm to 20 sccm, the grain sizes become smaller. The grain size is smallest when NH_3 and H_2 are both 100 sccm, and the film is smoother as revealed by AFM studies. The AFM images (Fig. 5) showed the rms roughness value (~4.8 nm) was ~15% of total film thickness (~33 nm) of as-deposited Co using 10 sccm NH_3. When the NH_3 flow increases to 100 sccm, the rms roughness (~0.7 nm) of as-deposited Co was ~5% of total film thickness (Fig. 5). When the NH_3 flow increases to 200 sccm, the film deposited without any H_2 has relatively larger grain sizes (Fig. 4) and higher roughness. The rms roughness value (~3.4 nm) of Co_3N was ~15% of the total thickness.

The step coverages for different growth conditions were examined by depositing CVD Co or Co_3N films on a silicon substrate with high aspect ratio holes (listed in Table 2). Then the coated substrate was hand cleaved to study the cross-section of the holes. The feed ratio of NH_3 and H_2 in the co-reactant gases was found to be an important factor affecting the growth rate and step coverage. The cobalt film grown with 100 sccm NH_3 and 100 sccm H_2 showed high conformality. The cross-sectional SEM images in Fig. 6(a) show cobalt films deposited conformally inside a hole with the aspect ratio ~48:1 (170 nm diameter and 8 μm depth). The cobalt thicknesses at the top, side wall and bottom of the feature are almost the same (18 nm), showing nearly 100% step coverage. Similarly, Co_xN showed excellent step coverage, covering ~45:1 aspect ratio holes uniformly, as shown in Fig. 6(b).

Table 3 Cobalt precursor solution flow rate (g h^{-1}), partial pressure of the cobalt precursor vapour inside the reactor (Pa), the growth rate of the cobalt film (nm min^{-1}), the derivative of the growth rate with respect to partial pressure (nm min^{-1} Pa^{-1}), the aspect ratio of the holes tested and the predicted step coverage

Solution flow rate (g h^{-1})	Co press. (Pa)	Growth rate, GR (nm min^{-1})	$\partial GR/\partial p$ (nm min^{-1} Pa^{-1})	Aspect ratio	Calc. step coverage
5	2.73	1.54	0.11	48	0.957
12.5	6.55	1.73	0.024	60	0.985
20	10.06	1.79	0.011	60	0.993

 This journal is © The Royal Society of Chemistry 2015

Published on 03 November 2015. Downloaded by Harvard University on 19/11/2015 15:08:36.

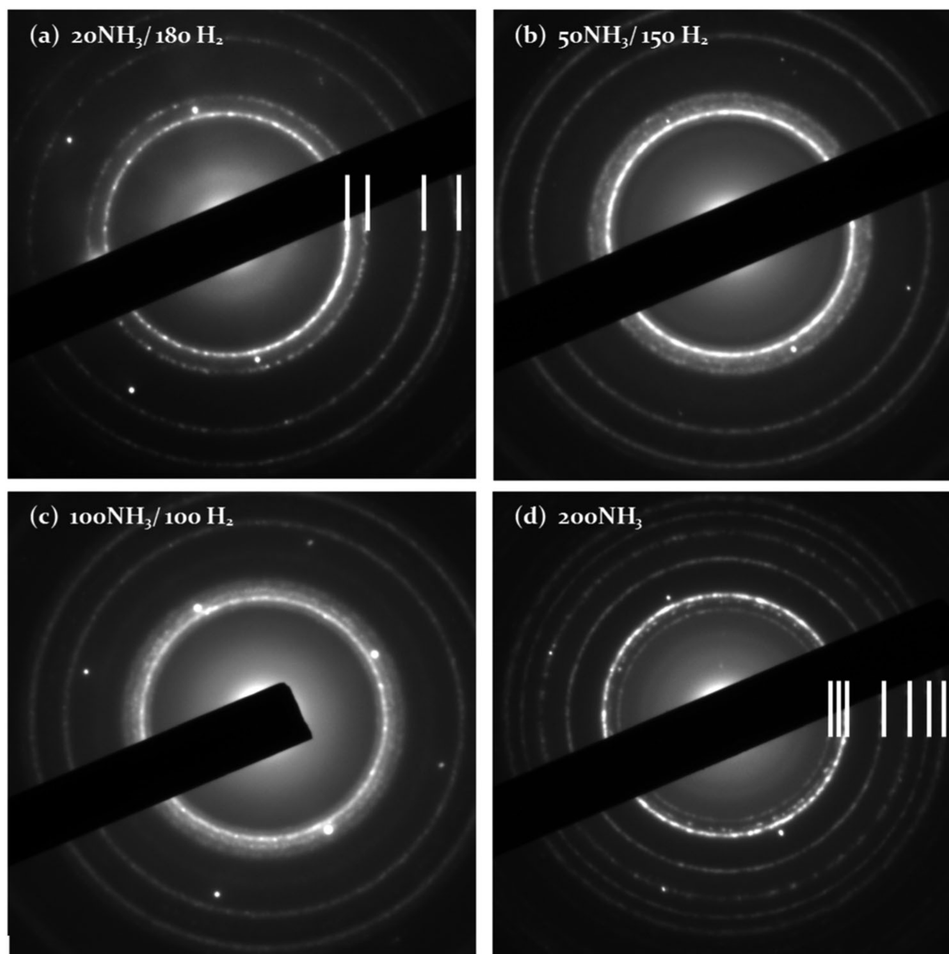

Fig. 3 Electron diffraction patterns of DLE-CVD Co_xN deposited with varied amounts of NH_3, H_2 as co-reactant on thermal oxide. (a) DLE-CVD Co deposited with NH_3/H_2 = 20/180 sccm. The diffraction rings (highlighted by white lines) belong to cubic Co (111), (200), (220), and (311), respectively. DLE-CVD Co deposited with (b) NH_3/H_2 = 50/150 sccm, (c) NH_3/H_2 = 100/100 sccm. (d) Co_3N deposited with 200 sccm NH_3. The diffraction rings (highlighted by white lines) belong to hexagonal Co_3N (100), (002), (101), (102), (110), (103), and (112), respectively.

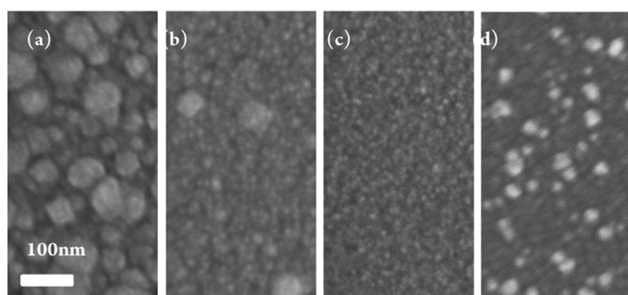

Fig. 4 Plane-view FESEM images for the as-deposited Co film at 200 °C with NH_3/H_2 = (a) 10 + 190, (b) 20 + 180, (c) 100 + 100 sccm, and Co_3N film using (d) 200 sccm NH_3 (figures shared the same scale bar).

Growth rate

Impact of the NH_3/H_2 feed ratio. The growth rate of the Co and Co_xN films under these conditions is around 1–2 nm min^{-1} (listed in Table 2). In the cases of using NH_3/H_2 = 10 + 190, 20 + 180, 50 + 150 or 150 + 50 sccm, the film growth rates are slightly higher than using 100 sccm NH_3 and 100 sccm H_2, while these films show less thickness uniformity along the flow direction and poorer step coverage. Thus the conditions of equal flow rates of ammonia and hydrogen were adopted for the remaining studies of CVD Co.

Impact of the delivery rate. Different delivery rates of cobalt precursor solution were tested to find out how the partial pressure of the cobalt precursor affects the deposition rate. Cobalt films were deposited at 200 °C with flow rates of carrier gas N_2, and reactant gases NH_3 and H_2 each set at 100 sccm, at a total pressure of 10 torr. The cobalt precursor solution was delivered at rates from 5 g h^{-1} to 20 g h^{-1}. When the precursor is delivered at 5 g h^{-1}, the film's sheet resistance is slightly higher than that of the film deposited with the delivery rate of 10 to 20 g h^{-1} (see ESI,† Fig. S3). This indicates the deposition rate is almost saturated at the precursor solution delivery rate of 5 g h^{-1}. Increasing the cobalt solution delivery rate above 5 g h^{-1} did not increase the cobalt growth rate much, as shown in ESI,† Fig. S3.

The saturation of DLE-CVD Co growth rate resulted in step coverage close to unity. According to Yanguas-Gil's model,[41,42]

Published on 03 November 2015. Downloaded by Harvard University on 19/11/2015 15:08:36.

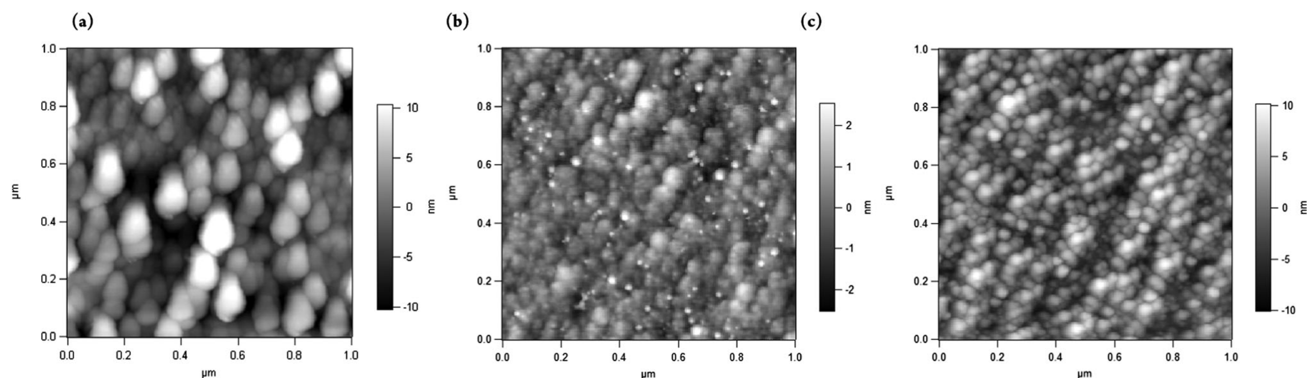

Fig. 5 AFM images of DLE-CVD Co and Co_3N deposited with varied amount of NH_3, H_2 as co-reactant on thermal oxide (a) 33 nm-Co deposited using 10 sccm NH_3 and 190 sccm H_2 (rms roughness = 4.8 nm); (b) 15 nm Co deposited using 100 sccm NH_3 and 100 sccm H_2 (rms roughness = 0.7 nm); (c) 22 nm Co_3N deposited with 200 sccm NH_3 (rms roughness = 3.4 nm).

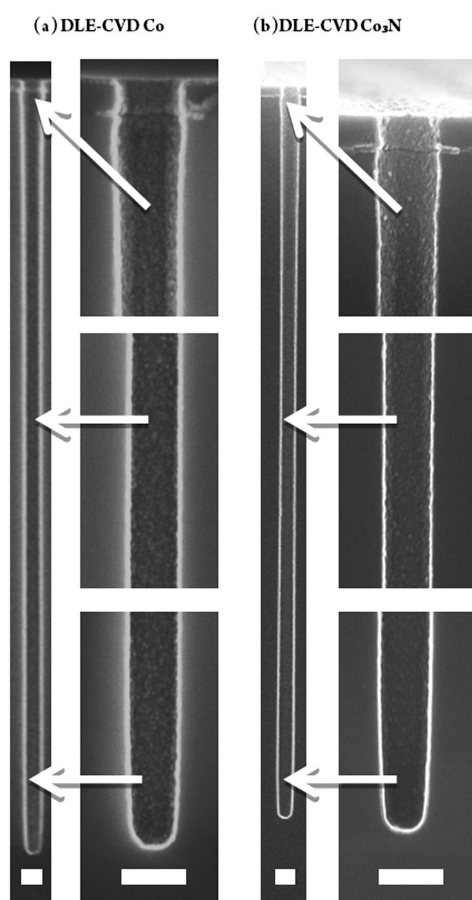

Fig. 6 Cross-sectional SEM images of DLE-CVD (a) Co film and (b) Co_3N film deposited at 200 °C on nanosized hole pattern. (a) ∼18 nm Co deposited with 100 sccm NH_3 and 100 sccm H_2 uniformly coating holes with 48 : 1 aspect ratio (170 nm diameter and 8.2 µm depth); (b) ∼10 nm Co_3N deposited with 200 sccm NH_3 uniformly coating holes with 45 : 1 aspect ratio (170 nm diameter and 7.6 µm depth). The white scale bar corresponds to 200 nm.

the step coverage (SC), defined as the ratio of the growth rate (GR) at the bottom of a trench or hole to the growth rate at the top (the opening), is given by

$$\mathrm{SC} = \frac{\text{Growth rate (bottom)}}{\text{Growth rate (top)}} = \frac{\mathrm{GR}(p-\Delta p, T)}{\mathrm{GR}(p, T)} = 1 - \frac{\partial \mathrm{GR}}{\partial p}\frac{c\rho k_\mathrm{B} T}{2D_\mathrm{o}}(\mathrm{AR})^2$$

where p is the precursor pressure at the opening, Δp is precursor pressure drop of the limiting precursor along the trench, $\partial GR/\partial p$ is the partial derivative of the growth rate with respect to the partial pressure of the limiting precursor, c is a geometric constant (c = 2 or 4 for a trench or a hole, respectively), p is the atomic density of the film, k_B is Boltzmann's constant, T is the substrate temperature, and $D_\mathrm{o} = \kappa\langle v_\mathrm{th}\rangle/3$, where $\langle v_\mathrm{th}\rangle$ is the average thermal velocity of the limiting precursor molecules and κ is a nondimensional constant of the order of 1.

In order to evaluate this formula for the step coverage, the growth rate for solution flow rates between 5 and 20 g h^{-1} were fit to the following functional form:

$$\mathrm{GR} = 1.91\ P/(P + 0.66)\ \mathrm{nm\ min^{-1}}$$

from which the pressure derivative is found to be

$$\partial\mathrm{GR}/\partial p = 1.26/(P + 0.66)^2\ \mathrm{nm\ min^{-2}\ Pa^{-1}}$$

Using these values the above formula predicts the values for step coverage shown in Table 3.

As the precursor pressure increases, the rate of change of the growth rate with pressure, $\partial\mathrm{GR}/\partial p$, becomes small, predicting very uniform film thickness inside holes, as well as along the gas flow in the reactor. For the experiment with 5 g h^{-1} of cobalt precursor solution, the thickness varies only slightly, as seen in Fig. 6. At a higher flow rate of 12.5 g h^{-1}, no deviation from uniform thickness can be seen in Fig. 7. These results demonstrate the capability of achieving excellent step coverage using the DLE-CVD method.

Temperature-dependence of growth rates. Cobalt films were deposited at various temperatures of 200 °C, 220 °C, 240 °C with NH_3/H_2 = 100/100 sccm, at 10 torr on thermal oxide. The growth rate increases as the deposition temperature rises. The amount

 This journal is © The Royal Society of Chemistry 2015

View Article Online

Published on 03 November 2015. Downloaded by Harvard University on 19/11/2015 15:08:36.

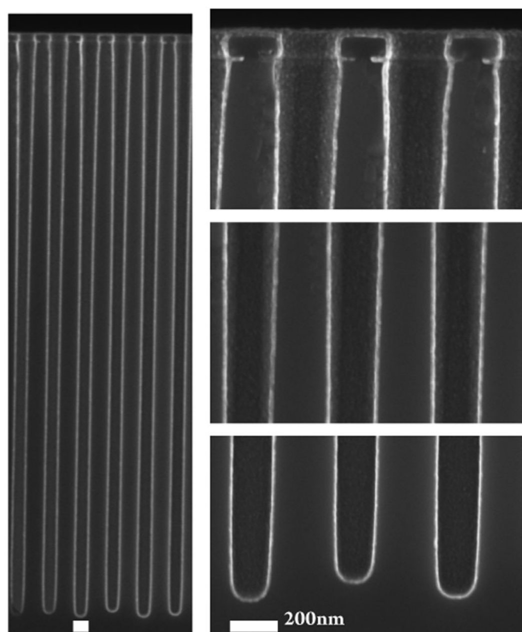

Fig. 7 Cross-sectional SEM images of DLE-CVD Co film deposited at 200 °C using 12.5 g h^{-1} cobalt precursor delivery rate on nanosized hole pattern. ~15 nm Co deposited using 100 sccm NH_3 and 100 sccm H_2 uniformly coated hole patterns with 60 : 1 aspect ratio (147 nm diameter and 8.8 μm depth).

of cobalt deposited was determined by XRF. An Arrhenius plot of the natural logarithm of the deposition rate and the reciprocal of temperature roughly follows a straight line, the slope of which implies the activation energy of 57 kJ mol^{-1} (see ESI,† Fig. S2). This value is much higher than the value 12 kJ mol^{-1} reported for a closely-related cobalt amidinate precursor, bis(*N-tert*-butyl-*N′*-ethylpropionamidinato)cobalt(II),[8] which reacts at lower deposition temperatures. For comparison, higher activation energies were reported for other cobalt precursors $CoCp(CO)_2$,[14] ($Co(acac)_2$),[12] and $CoNO(CO)_3$:[13,32] 68 kJ mol^{-1}, 70 kJ mol^{-1} and 160 kJ mol^{-1}, respectively.

Conclusions

We used direct-liquid-evaporation chemical vapor deposition (DLE-CVD) processes to produce smooth cobalt and cobalt nitride films with excellent step coverage at a low temperature of 200 °C. DLE-CVD Co and Co_xN films have much higher growth rates compared to those fabricated by atomic layer deposition (ALD) processes, but still provide uniform thicknesses inside narrow holes. Additionally, the DLE-CVD method can avoid particle formation and blockage problems shown by the DLI-CVD method. The use of ammonia in addition to H_2 promotes pure cobalt growth at a temperature of 200 °C. Co thin films were deposited by the reduction of bis(*N,N′*-diisopropylacetamidinato)cobalt(II) using a mixture of NH_3 and H_2. DLE-CVD cobalt films deposited using 100 sccm NH_3 and 100 sccm H_2 were found to have the lowest roughness, most uniform thickness along the gas flow direction, highest step coverage and highest conductivity compared to films made using other NH_3/H_2 feed ratios. The Co films formed a cubic phase, with a low resistivity of ~28 μΩ cm for 45 nm thick film, uniformly coating trenches with 60 : 1 aspect ratio. Cobalt nitride films were deposited by using ammonia as the only co-reactant. Co_3N showed a hexagonal phase, uniformly covering trenches with a 45 : 1 aspect ratio. These results show that the DLE-CVD method is valuable for high-throughput deposition of pure and conformal Co and Co_3N thin films at low temperatures.

Acknowledgements

The authors thank Dr Qing Min Wang, Dr Jean-Sebastien Lehn, Dr Huazhi Li and Dr Deo Shenai for helpful discussions. The cobalt amidinate precursor was supplied by their work at Dow Chemical Company. Tokyo Electron provided silicon substrates with narrow holes. This work was performed in part at the Center for Nanoscale Systems (CNS) at Harvard University, a member of the National Nanotechnology Infrastructure Network (NNIN), which was supported by NSF award no. ECS-0335765.

Notes and references

1 S. S. P. Parkin, N. More and K. P. Roche, *Phys. Rev. Lett.*, 1990, **64**, 2304–2307.
2 A. E. Berkowitz, J. R. Mitchell, M. J. Carey, A. P. Young, S. Zhang, F. E. Spada, F. T. Parker, A. Hutten and G. Thomas, *Phys. Rev. Lett.*, 1992, **68**, 3745–3748.
3 C. T. Black, C. B. Murray, R. L. Sandstrom and S. Sun, *Science*, 2000, **290**, 1131–1134.
4 D. Chiba, S. Fukami, K. Shimamura, N. Ishiwata, K. Kobayashi and T. Ono, *Nat. Mater.*, 2011, **10**, 853–856.
5 B. S. Lim, A. Rahtu and R. G. Gordon, *Nat. Mater.*, 2003, **2**, 749–754.
6 Z. Li, R. G. Gordon, D. B. Farmer, Y. Lin and J. Vlassak, *Electrochem. Solid-State Lett.*, 2005, **8**, G182–G185.
7 H. B. Bhandari, J. Yang, H. Kim, Y. Lin, R. G. Gordon, Q. M. Wang, J.-S. M. Lehn, H. Li and D. Shenai, *ECS J. Solid State Sci. Technol.*, 2012, **1**, N79–N84.
8 H. Shimizu, Y. Suzuki, T. Nogami, N. Tajima, T. Momose, Y. Kobayashi and Y. Shimogaki, *ECS J. Solid State Sci. Technol.*, 2013, **2**, P311–P315.
9 H. Shimizu, A. Kumamoto, K. Shima, Y. Kobayashi, T. Momose, T. Nogami and Y. Shimogaki, *ECS J. Solid State Sci. Technol.*, 2013, **2**, P471–P477.
10 Y. Kokaze, S. Kodaira, Y. Endo, J. Hamaguchi, M. Harada, S. Kumamoto, Y. Sakamoto and Y. Higuchi, *Jpn. J. Appl. Phys.*, 2013, **52**, 05FA01.
11 G. J. M. Dormans, G. J. B. M. Meekes and E. G. J. Staring, *J. Cryst. Growth*, 1991, **114**, 364–372.
12 P. A. Premkumar, N. Bahlawane and K. Kohse-Höinghaus, *Chem. Vap. Deposition*, 2007, **13**, 219–226.
13 P. A. Lane, P. E. Oliver, P. J. Wright, C. L. Reeves, A. D. Pitt and B. Cockayne, *Chem. Vap. Deposition*, 1998, **4**, 183–186.

Published on 03 November 2015. Downloaded by Harvard University on 19/11/2015 15:08:36.

14 M. F. Chioncel and P. W. Haycock, *Chem. Vap. Deposition*, 2005, **11**, 235–243.
15 J. Lee, H. J. Yang, J. H. Lee, J. Y. Kim, W. J. Nam, H. J. Shin, Y. K. Ko, J. G. Lee, E. G. Lee and C. S. Kim, *J. Electrochem. Soc.*, 2006, **153**, G539–G542.
16 N. Bahlawane, P. Antony Premkumar, K. Onwuka, K. Rott, G. Reiss and K. Kohse-Höinghaus, *Surf. Coat. Technol.*, 2007, **201**, 8914–8918.
17 P. A. Premkumar, A. Turchanin and N. Bahlawane, *Chem. Mater.*, 2007, **19**, 6206–6211.
18 C. Georgi, A. Hildebrandt, T. Waechtler, S. E. Schulz, T. Gessner and H. Lang, *J. Mater. Chem. C*, 2014, **2**, 4676–4682.
19 H.-B.-R. Lee and H. Kim, *Electrochem. Solid-State Lett.*, 2006, **9**, G323–G325.
20 H.-B.-R. Lee, W.-H. Kim, J. W. Lee, J.-M. Kim, K. Heo, I. C. Hwang, Y. Park, S. Hong and H. Kim, *J. Electrochem. Soc.*, 2010, **157**, D10–D15.
21 H. Shimizu, K. Sakoda, T. Momose, M. Koshi and Y. Shimogaki, *J. Vac. Sci. Technol., A*, 2012, **30**, 01A144–147.
22 International Technology Roadmap for Semiconductors, http://www.itrs.net/Links/2012ITRS/Home2012.htm.
23 Z. Li, R. G. Gordon, V. Pallem, H. Li and D. V. Shenai, *Chem. Mater.*, 2010, **22**, 3060–3066.
24 C. J. Anthony and R. C. Paul, *J. Phys. D: Appl. Phys.*, 2003, **36**, R80.
25 Z. Li, R. G. Gordon, H. Li, D. V. Shenai and C. Lavoie, *J. Electrochem. Soc.*, 2010, **157**, H679–H683.
26 L. M. Apátiga and V. M. Castaño, *Thin Solid Films*, 2006, **496**, 576–579.
27 L. Gao, P. Härter, C. Linsmeier, J. Gstöttner, R. Emling and D. Schmitt-Landsiedel, *Mater. Sci. Semicond. Process.*, 2004, **7**, 331–335.
28 S. K. Dey, J. Goswami, A. Das, W. Cao, M. Floyd and R. Carpenter, *J. Appl. Phys.*, 2003, **94**, 774–777.
29 D. Bollmann, R. Merkel and A. Klumpp, *Microelectron. Eng.*, 1997, **37–38**, 105–110.
30 C. Dubourdieu, H. Roussel, C. Jimenez, M. Audier, J. P. Sénateur, S. Lhostis, L. Auvray, F. Ducroquet, B. J. O'Sullivan, P. K. Hurley, S. Rushworth and L. Hubert-Pfalzgraf, *Mater. Sci. Eng., B*, 2005, **118**, 105–111.
31 Z. G. Xiao, *Rev. Sci. Instrum.*, 2003, **74**, 3879–3880.
32 A. R. Ivanova, G. Nuesca, X. Chen, C. Goldberg, A. E. Kaloyeros, B. Arkles and J. J. Sullivan, *J. Electrochem. Soc.*, 1999, **146**, 2139–2145.
33 Y. K. Ko, D. S. Park, B. S. Seo, H. J. Yang, H. J. Shin, J. Y. Kim, J. H. Lee, W. H. Lee, P. J. Reucroft and J. G. Lee, *Mater. Chem. Phys.*, 2003, **80**, 560–564.
34 Z. Li, D. K. Lee, M. Coulter, L. N. J. Rodriguez and R. G. Gordon, *Dalton Trans.*, 2008, 2592–2597.
35 B. S. Lim, A. Rahtu, J.-S. Park and R. G. Gordon, *Inorg. Chem.*, 2003, **42**, 7951–7958.
36 E. T. Hunde and J. J. Watkins, *Chem. Mater.*, 2004, **16**, 498–503.
37 J. Wu, J. Li, C. Zhou, X. Lei, T. Gaffney, J. A. T. Norman, Z. Li, R. Gordon and H. Cheng, *Organometallics*, 2007, **26**, 2803–2805.
38 T. Fauster, G. Rangelov, J. Stober and B. Eisenhut, *Phys. Rev. B: Condens. Matter Mater. Phys.*, 1993, **48**, 11361–11366.
39 C. Rath, J. E. Prieto, S. Müller, R. Miranda and K. Heinz, *Phys. Rev. B: Condens. Matter Mater. Phys.*, 1997, **55**, 10791–10799.
40 M. T. Kief and W. F. Egelhoff, Jr., *Phys. Rev. B: Condens. Matter Mater. Phys.*, 1993, **47**, 10785–10814.
41 A. Yanguas-Gil, Y. Yang, N. Kumar and J. R. Abelson, *J. Vac. Sci. Technol., A*, 2009, **27**, 1235–1243.
42 A. Yanguas-Gil, N. Kumar, Y. Yang and J. R. Abelson, *J. Vac. Sci. Technol., A*, 2009, **27**, 1244–1248.

 This journal is © The Royal Society of Chemistry 2015